

Nonpolar m -plane $\text{Al}_x\text{Ga}_{1-x}\text{N}$ layers grown on $(10\bar{1}0)$ sapphire by MOVPE

Duc V. Dinh,^{1, a)} Hiroshi Amano,^{1, 2} and Markus Pristovsek¹

¹⁾*Institute of Materials and Systems for Sustainability, Nagoya University, Nagoya 464-8601, Japan*

²⁾*Akasaka Research Center, Nagoya University, Nagoya 464-8603, Japan*

(Dated: 12 October 2018)

Heteroepitaxial growth of single-phase nonpolar $(10\bar{1}0)$ m -plane $\text{Al}_x\text{Ga}_{1-x}\text{N}$ layers on m -plane sapphire substrates was investigated by metalorganic vapour phase epitaxy. Different Al/Ga gas phase ratios were used to adjust the AlN mole fraction over the entire range of composition. All m -plane AlGa_N layers show an orthorhombic distortion in the wurtzite unit cell due to anisotropic in-plane strain. This distortion decreases with increasing the AlN mole fraction due to a decreased anisotropic biaxial strain. The AlN mole fraction of m -plane layers and c -plane co-loaded layers estimated by X-ray diffraction is comparable. This is consistent with their comparable energy bandgaps estimated from room-temperature dielectric functions. The dependence of the energy bandgap on composition indicates a bowing parameter of 0.9 eV.

Keywords: A1. Crystal morphology, A3. Metalorganic vapour phase epitaxy, B1. Nitrides, B2. AlGa_N, B2. Semiconducting aluminium compounds

I. INTRODUCTION

Group III-nitride semiconductor compounds (e.g., AlN, GaN and InN) have attracted much attention for application in optoelectronic devices, in particular ultraviolet (UV) and visible light-emitting diodes (LEDs). UV LEDs epitaxially grown along the $[0001]$ polar axis has strong polarization fields across the quantum-well (QW). These fields reduce the electron-hole wavefunction overlap resulting in a reduction of the radiative recombination rate. This reduction together with a high resistivity of n-/p-doped AlGa_N layers hinder the performance of devices operating at below 350 nm . Additionally, for wavelengths shorter than $\sim 250\text{ nm}$ the light emission mode changes from transverse electric polarization ($E \perp [0001]$) to transverse magnetic polarization ($E \parallel [0001]$), which reduces light extraction². Growth on nonpolar $(11\bar{2}0)$ a -plane and $(10\bar{1}0)$ m -plane results in built-in field free³, which should increase the radiative recombination efficiency of nonpolar QW active region.

Absorption of the UV light also strongly reduces the performance of UV LEDs. Therefore, highly transparent AlGa_N and AlN templates are required, which must also have good material quality if the potential benefits to the device performance are to be realized. Growth and characterization of nonpolar and semipolar Al(Ga)_N structures have been homoepitaxially grown on high-quality nonpolar a -plane⁴ and m -plane AlN^{5,6}, as well as semipolar $(10\bar{1}2)$ ^{7,8} and $(20\bar{2}1)$ AlN⁹ bulk substrates using metalorganic vapour phase epitaxy (MOVPE). Despite their high crystalline quality, these substrates are small, expensive, and UV-transparency still remains a challenge^{10,11}.

For commercial nitride-based emitters, sapphire substrates have commonly been used due to their large di-

ameter wafer sizes, low-cost and visible/UV light transparency. However, for nonpolar nitride layers heteroepitaxially grown on planar sapphire substrates, a high density of threading dislocations and basal-plane stacking faults (BSFs) generates at the layer/sapphire interface due to their lattice mismatch^{12,13}. This high density strongly reduces the efficiency of UV LEDs^{1,14}. Recently, high-temperature thermal annealing was used to improve the material and optical properties of a -plane AlN^{15,16} and m -plane AlN^{17,18}.

MOVPE-grown AlGa_N layers grown on sapphire substrates with different surface orientations have already been reported, e.g., a -plane¹⁹, c -plane²⁰⁻²³ and $(11\bar{2}2)$ ²⁴⁻²⁶. However, so far there is no report on growth of m -plane AlGa_N on sapphire. The most possible reason is due to the lack of m -plane AlN templates. Recently, we have demonstrated growth of single phase m -plane AlN templates on m -plane sapphire¹⁸.

In this paper, we report on MOVPE-growth of m -plane $\text{Al}_x\text{Ga}_{1-x}\text{N}$ layers on m -plane sapphire substrates over the entire range of composition. The crystallinity, surface morphology, and optical energy bandgap of the layers were investigated as a function of the AlN mole fraction (x_{AlN}).

II. EXPERIMENTAL

Growth was performed on 2-in. $(10\bar{1}0)$ m -plane sapphire wafers in an EpiQuest 3×2 -in. close-coupled showerhead MOVPE reactor. Ammonia (NH_3), trimethylgallium (TMGa) and trimethylaluminium (TMAI) were used as precursors. Under a reactor pressure of 27 mbar in a hydrogen ambient, the wafers were heated to 900°C to produce an AlN nucleation layer ($\sim 20\text{ nm}$ thick) with an NH_3 partial pressure (P_{NH_3}) of 12.44 Pa and $P_{\text{TMAI}} = 0.164\text{ Pa}$. Afterwards, the samples were heated to 1050°C to grow a 100-nm-thick AlN layer at a reactor pressure of 100 mbar ($P_{\text{NH}_3} = 6.22\text{ Pa}$, $P_{\text{TMAI}} = 0.164\text{ Pa}$).

^{a)}Electronic mail: duc.vn.dinh@gmail.com

$\text{Al}_x\text{Ga}_{1-x}\text{N}$ layers with a nominal thickness of $1.5\ \mu\text{m}$ (estimated from ellipsometry data) were subsequently grown on the AlN templates at the same temperature and pressure. To vary x_{AlN} of $\text{Al}_x\text{Ga}_{1-x}\text{N}$ over the entire range of composition, different $R_{\text{AlGaN}} = \text{TMAI}/(\text{TMAI} + \text{TMGa})$ gas phase ratios were employed while P_{NH_3} was kept constant of 333.3 Pa. For R_{AlGaN} ranging from 0.1 to 0.7, P_{TMAI} was fixed at 0.614 Pa, while P_{TMGa} was varied from 0.363 to 5.587 Pa. For $R_{\text{AlGaN}} = 0.8$, P_{TMAI} and P_{TMGa} of 1.458 and 0.363 Pa were used, respectively. For comparison, c -plane AlGaN layers were also simultaneously grown on c -plane sapphire wafers.

The crystal orientation and properties of the samples were characterized using a PANalytical X'pert triple-axis high-resolution X-ray diffraction (XRD) system with a $\text{CuK}\alpha_1$ source. Symmetric $(10\bar{1}0)$ X-ray rocking curves (XRCs) of the layers were measured using an open detector without any receiving slit. The surface morphology of the samples was measured by atomic force microscopy (AFM) in tapping mode (Nanocute, SII NanoTech). The fundamental bandgap of the layers were estimated from real and imaginary parts of dielectric functions DFs. DFs were recorded at room temperature using a Horiba UVISEL 2 spectroscopic ellipsometer at an incident angle of 70° and a spot size of $2030 \times 705\ \mu\text{m}^2$. The photon energy was varied from 1.45 to 6.45 eV with the spectral resolution of 20 meV.

III. RESULTS AND DISCUSSION

Fig. 1(a) shows symmetric ω - 2θ XRD scans of AlGaN layers grown on m -plane sapphire with R_{AlGaN} of 0.0, 0.6, and 1.0. Besides the $(30\bar{3}0)$ reflection of sapphire at 34.1° , there are only the $(10\bar{1}0)$, $(20\bar{2}0)$ and $(30\bar{3}0)$ reflections related to m -plane AlGaN. Fig. 1(b) shows symmetric $(10\bar{1}0)$ XRC FWHM values of three m -plane AlGaN layers measured as a function of azimuthal angle. The FWHM value along $[0001]_{\text{AlGaN}}$ is larger than $[11\bar{2}0]_{\text{AlGaN}}$, attributed to effects of BSFs^{12,13}. These values increase with increasing x_{AlN} indicating a decreased crystallinity. This is consistent with previous works reported for a -plane AlGaN¹⁹ and $(11\bar{2}2)$ AlGaN²⁵.

The in-plane epitaxial relationship between the m -plane AlGaN layers and m -plane sapphire substrates has also been investigated. Azimuthal scans of the $\{11\bar{2}0\}_{\text{AlGaN}}$ and $\{20\bar{2}4\}_{\text{sapphire}}$ reflections were measured. The relationship is found to be $[0001]_{\text{AlGaN}} \parallel [11\bar{2}0]_{\text{sapphire}}$ and $[11\bar{2}0]_{\text{AlGaN}} \parallel [0001]_{\text{sapphire}}$. A schematic diagram of this relationship is shown in the inset of Fig. 2(a).

For nonpolar AlGaN layers hetero-epitaxially grown on m -plane and r -plane sapphire substrates, the anisotropy (along two orthogonal in-plane directions) in the lattice and thermal mismatches between the layers and substrates leads to an orthorhombic deformation of the wurtzite unit cell. This makes lattice parameter measure-

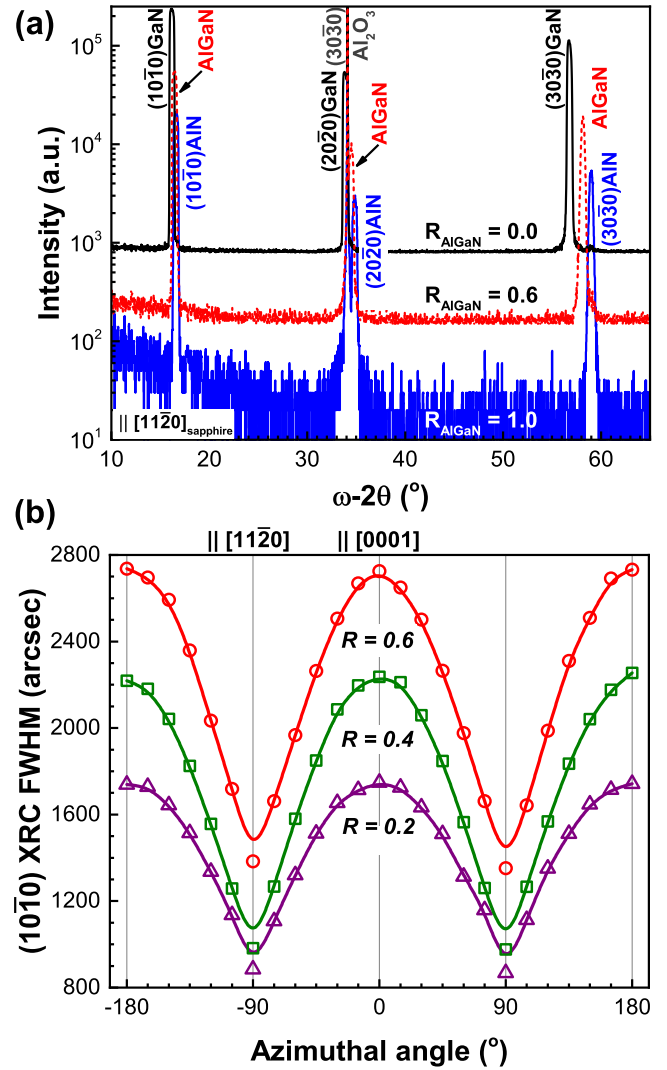


FIG. 1. (a) Symmetric ω - 2θ XRD scans of AlGaN layers grown on m -plane sapphire substrates with different R_{AlGaN} ratios. (b) Symmetric $(10\bar{1}0)$ XRC FWHM of three selected AlGaN layers plotted as a function of azimuthal angle.

ments, and thus x_{AlN} determination, difficult. Laskar et al. have previously developed a method to calculate lattice parameters for a -plane AlGaN grown on r -plane sapphire²⁷. This method has already been applied to calculate lattice deformation of m -plane AlN layers grown on m -plane sapphire^{17,18}.

For the m -plane AlGaN samples studied here, their in-plane and off-plane a lattice constants, as well as in-plane c -axis lattice constants were calculated from 2θ measurements of nine different symmetric, skew-symmetric and asymmetric AlGaN reflections including $(10\bar{1}0)$, $(10\bar{1}1)$, $(11\bar{2}0)$, $(11\bar{2}2)$, $(12\bar{3}0)$, $(20\bar{2}1)$, $(\bar{2}021)$, $(21\bar{3}1)$ and $(21\bar{3}3)$. Fig. 3 shows the measured lattice constants of the layers as a function of R_{AlGaN} . All the lattice constants show a linear behaviour with R_{AlGaN} . Additionally, all the layers are almost relaxed along $[11\bar{2}0]_{\text{AlGaN}}$, while they are

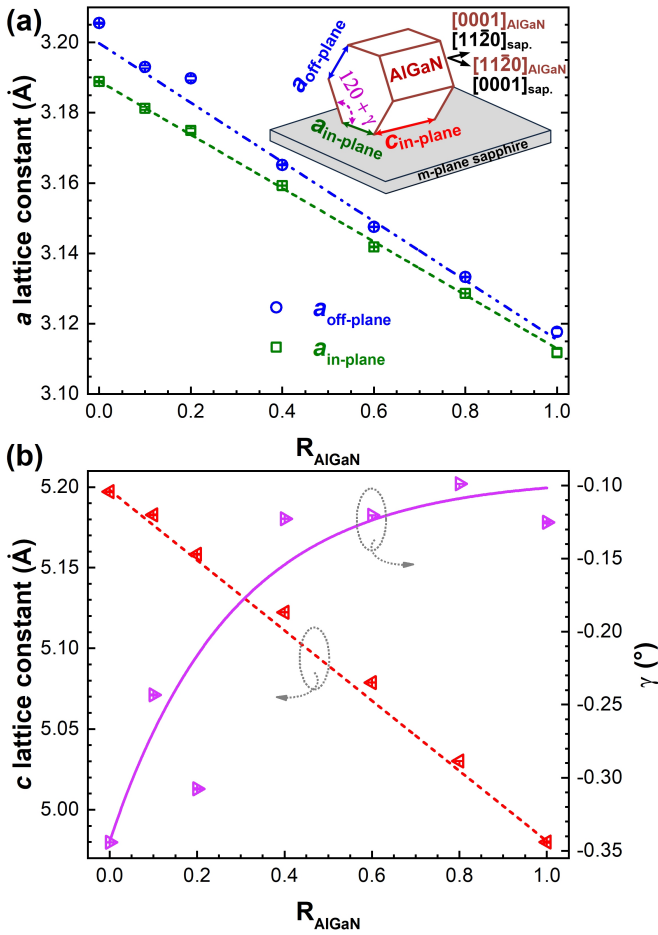


FIG. 2. (a) Measured in-plane and off-plane a lattice constants, as well as (b) in-plane c lattice constant of the MOVPE-grown m -plane $\text{Al}_x\text{Ga}_{1-x}\text{N}$ layers grown with different R_{AlGaN} . The *inset* in (a) shows a schematic diagram of the in-plane relationship between m -plane AlGaN and m -plane sapphire.

tensile stressed along $[0001]_{\text{AlGaN}}$. This tension decreases from 0.21 to 0.02 with increasing x_{AlN} .

All the m -plane AlGaN layers have been found to be distorted with an angle (γ) that increases from about -0.34° to -0.10° with increasing R_{AlGaN} . This increase corresponds to a decreased off-plane a lattice constant, indicating a decreased anisotropic biaxial strain between the layers and the AlN interlayers. This is plausible due to a reduced lattice mismatch of AlGaN with respect to AlN as R_{AlGaN} (x_{AlN}) $\rightarrow 1$. Based on these measured lattice constants, x_{AlN} of the layers has been estimated. As shown in Fig. 3, x_{AlN} linearly increases with increasing R_{AlGaN} . This linear behaviour indicates minimum gas phase pre-reactions of the group-III precursors and NH_3 ^{22,28}.

For c -plane AlGaN reference layers, x_{AlN} was calculated based on in-plane a and off-plane c lattice constants, determined by different reflections including (0002), (0004), (0006), (10 $\bar{1}$ 2), (10 $\bar{1}$ 5) and (11 $\bar{2}$ 2). The

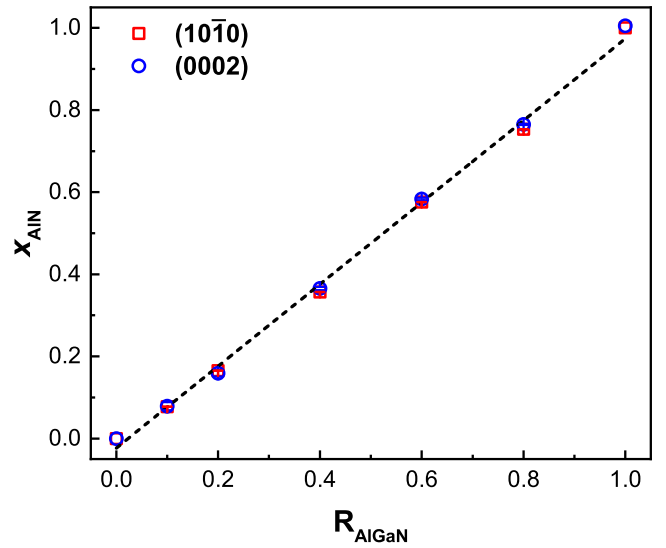


FIG. 3. Estimated x_{AlN} from XRD data of the m -plane and c -plane AlGaN co-loaded layers as a function of $R_{\text{AlGaN}} = \text{TMAI}/(\text{TMAI} + \text{TMGa})$.

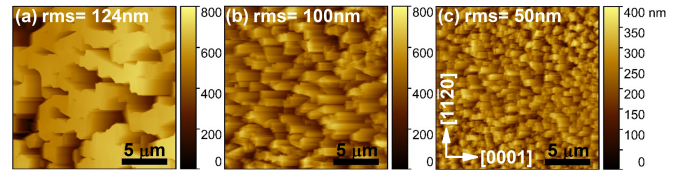


FIG. 4. $20 \times 20 \mu\text{m}^2$ AFM images of three selected m -plane AlGaN layers with x_{AlN} of (a) 0.165, (b) 0.357, and (c) 0.576. Root-mean square (rms) roughness values of these layers are shown for comparison.

x_{AlN} values of the c -plane and m -plane layers are comparable as shown in Fig. 3. This result is slightly different compared to a -plane and c -plane AlGaN layers¹⁹, whereas a slightly lower x_{AlN} of a -plane layers than that of c -plane layers was found.

Fig. 4 shows $20 \times 20 \mu\text{m}^2$ AFM images of three m -plane AlGaN layers with $x_{\text{AlN}} = 0.165$, 0.357, and 0.576. Grain size of the layers monotonically decreases with increasing x_{AlN} , from about 5 μm to 2 μm and about 4 μm to 1 μm along $[0001]_{\text{AlGaN}}$ and $[11\bar{2}0]_{\text{AlGaN}}$, respectively. This can be explained by the lower surface mobility and larger sticking coefficient of Al atoms compared to those of Ga atoms. The roughening (and thus the origin of grains) occurs likely when the layers start to be relaxed. Even though, the strain is higher for the layers with lower x_{AlN} , the longer migration length will lead to their coalescence.

The larger grain size along $[0001]_{\text{AlGaN}}$ than $[11\bar{2}0]_{\text{AlGaN}}$ is attributed to a longer diffusion length of Al and Ga atoms along $[0001]$ ²⁹. Despite this, the XRC FWHM value along $[0001]$ is larger than that along $[11\bar{2}0]$. This indicates dominant effects of BSFs causing the broadening of the (10 $\bar{1}$ 0) reflection along $[0001]$ ^{12,13}.

Fig. 5(a) shows real ($\langle \epsilon_1 \rangle$) and imaginary ($\langle \epsilon_2 \rangle$)

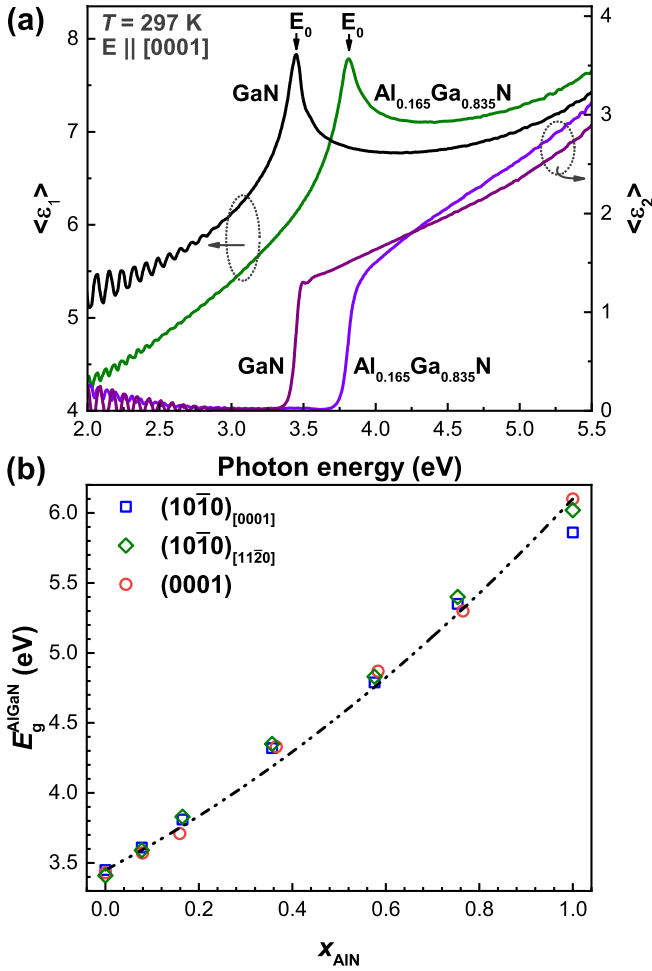


FIG. 5. (a) Real ($\langle\epsilon_1\rangle$) and imaginary ($\langle\epsilon_2\rangle$) parts of DFs measured along $[0001]_{\text{AlGaIn}}$ of m -plane GaN and $\text{Al}_{0.165}\text{Ga}_{0.835}\text{N}$ layers grown on m -plane sapphire. Bandgap (E_0) of the band structure is indicated by arrows. (b) Bandgap of the m -plane and c -plane AlGaIn co-loaded layers plotted as a function of x_{AlIn} . The dashed line is a bandgap-bowing fitting of the experimental data with a bowing parameter of 0.9 eV.

parts of the effective DFs measured along $[0001]_{\text{AlGaIn}}$ of m -plane GaN and $\text{Al}_{0.165}\text{Ga}_{0.835}\text{N}$ layers grown on m -plane sapphire. From these parts, the fundamental energy bandgap (i.e., the optical transition from the Γ_9^v valence band into the Γ_{7+}^c conduction band) of these layers is estimated from a sharp E_0 peak^{5,30}. For example, E_g^{GaN} and E_g^{AlGaIn} of the m -plane GaN and $\text{Al}_{0.165}\text{Ga}_{0.835}\text{N}$ were estimated to be 3.45 and 3.81 eV, respectively. It should be noted that the intensity and sharpness of E_0 become worse with increasing x_{AlIn} , attributed to the lower material quality of the layers. Interference fringes due to reflection at the AlGaIn/AlN/sapphire interface can be observed below the bandgap. The interference fringes of all m -plane layers are very weak (even become unobservable) because of rough interfaces. In contrast, pronounced fringes have

been observed for all c -plane reference samples due to their smooth surface morphology ($\text{rms} \leq 5$ nm, estimated from $20 \times 20 \mu\text{m}^2$ scan areas).

Birefringence has been also investigated for the m -plane layers. A small difference (i.e., the crystal field splitting energy Δ_{cf}) in E_g^{AlGaIn} has been found, where E_g^{AlGaIn} along $[11\bar{2}0]$ is slightly larger than along $[0001]$ as shown in Fig. 5(b). This is attributed to a different transition from Γ_9^v to Γ_{7-}^c and Γ_{7+}^c , respectively^{5,23,26}. Δ_{cf} is estimated to be about 0.04 eV and -0.16 eV for m -plane GaN and AlN layers, respectively. Additionally, crystal field splitting energy increases with increasing x_{AlIn} , e.g., $\Delta_{\text{cf}} = 0.02$ eV and 0.05 eV estimated for the layers with $x_{\text{AlIn}} = 0.165$ and 0.754, respectively. When introducing a bowing parameter b_{cf} to fit the Δ_{cf} data, a $b_{\text{cf}} = (-0.1 \pm 0.06)$ eV has been found. This is comparable with values reported for c -plane AlGaIn layers^{23,31}; however, this is larger than a value reported for $(11\bar{2}2)$ layers²⁶.

E_g^{AlGaIn} of the m -plane and c -plane AlGaIn layers is plotted as a function of x_{AlIn} in Fig. 5(b). Their E_g^{AlGaIn} values are comparable. This indicates a comparable x_{AlIn} , consistent with the results estimated by XRD as shown in Fig. 3. The dependence of E_g^{AlGaIn} on x_{AlIn} can be described by the relation:

$$E_g^{\text{Al}_x\text{Ga}_{1-x}\text{N}} = x \cdot E_g^{\text{AlN}} + (1-x) \cdot E_g^{\text{GaN}} - b \cdot x \cdot (1-x),$$

where b denotes the bowing parameter. The shift of E_g^{AlGaIn} with x_{AlIn} is well reproduced with a bowing parameter of $b = (0.9 \pm 0.1)$ eV. This value is in good agreement with a value reported for a -plane AlGaIn layers¹⁹, $(11\bar{2}2)$ AlGaIn²⁶, as well as values reported for c -plane AlGaIn layers^{23,30-32}.

IV. CONCLUSIONS

MOVPE-growth of m -plane $\text{Al}_x\text{Ga}_{1-x}\text{N}$ layers on m -plane sapphire substrates has been investigated over the entire range of composition. An orthorhombic distortion has been found for all m -plane layers. This distortion decreases with increasing the AlN mole fraction due to a decreased anisotropic biaxial strain. The AlN mole fraction of m -plane layers and c -plane co-loaded layers estimated by X-ray diffraction is comparable, consistent with their comparable bandgaps estimated from room-temperature dielectric functions. The dependence of the energy bandgap on composition indicates a bowing parameter b of 0.9 eV. The crystal field energy Δ_{cf} is found to change between the values for GaN and AlN with a bowing parameter b_{cf} of about -0.1 eV.

ACKNOWLEDGMENTS

We gratefully acknowledge facilities support from the Center for Integrated Research of Future Electronics-Transformative Electronics Facilities (C-TEFs), Institute of Materials and Systems for Sustainability (IMaSS) of Nagoya University.

REFERENCES

- ¹M. Kneissl, T. Kolbe, C. Chua, V. Kueller, N. Lobo, J. Stellmach, A. Knauer, H. Rodriguez, S. Einfeldt, Z. Yang, N. M. Johnson, M. Weyers, *Semicond. Sci. Technol.* 26 (1) (2011) 014036. doi:10.1088/0268-1242/26/1/014036.
- ²J. E. Northrup, C. L. Chua, Z. Yang, T. Wunderer, M. Kneissl, N. M. Johnson, T. Kolbe, *Appl. Phys. Lett.* 100 (2) (2012) 021101–4. doi:10.1063/1.3675451.
- ³T. Takeuchi, S. Sota, M. Katsuragawa, M. Komori, H. Takeuchi, H. Amano, I. Akasaki, *Jpn. J. Appl. Phys.* 36 (4A) (1997) L382. doi:10.1143/JJAP.36.L382.
- ⁴A. Sedhain, N. Nepal, M. L. Nakarmi, T. M. Al tahtamouni, J. Y. Lin, H. X. Jiang, Z. Gu, J. H. Edgar, *Appl. Phys. Lett.* 93 (4) (2008) 041905–3. doi:10.1063/1.2965613.
- ⁵M. Feneberg, M. F. Romero, M. Röpписcher, C. Cobet, N. Esser, B. Neuschl, K. Thonke, M. Bickermann, R. Goldhahn, *Phys. Rev. B* 87 (23) (2013) 235209. doi:10.1103/PhysRevB.87.235209.
- ⁶I. Bryan, Z. Bryan, M. Bobea, L. Hussey, R. Kirste, R. Collazo, Z. Sitar, *J. Appl. Phys.* 116 (13) (2014) 133517–5. doi:10.1063/1.4897233.
- ⁷S. Ichikawa, Y. Iwata, M. Funato, S. Nagata, Y. Kawakami, *Appl. Phys. Lett.* 104 (25) (2014) 252102–4. doi:10.1063/1.4884897.
- ⁸R. Akaike, S. Ichikawa, M. Funato, Y. Kawakami, *Appl. Phys. Express* 11 (6) (2018) 061001. doi:10.7567/APEX.11.061001.
- ⁹T. Wunderer, Z. Yang, M. Feneberg, M. Batres, M. Teepe, N. Johnson, *Appl. Phys. Lett.* 111 (11) (2017) 111101–3. doi:10.1063/1.4985156.
- ¹⁰R. Collazo, J. Xie, B. E. Gaddy, Z. Bryan, R. Kirste, M. Hoffmann, R. Dalmau, B. Moody, Y. Kumagai, T. Nagashima, Y. Kubota, T. Kinoshita, A. Koukitu, D. L. Irving, Z. Sitar, *Appl. Phys. Lett.* 100 (19) (2012) 191914–5. doi:10.1063/1.4717623.
- ¹¹D. Alden, J. S. Harris, Z. Bryan, J. N. Baker, P. Reddy, S. Mita, G. Callsen, A. Hoffmann, D. L. Irving, R. Collazo, Z. Sitar, *Phys. Rev. Appl.* 9 (5) (2018) 054036. doi:10.1103/PhysRevApplied.9.054036.
- ¹²M. B. McLaurin, A. Hirai, E. Young, F. Wu, J. S. Speck, *Jpn. J. Appl. Phys.* 47 (7R) (2008) 5429. doi:10.1143/JJAP.47.5429.
- ¹³M. A. Moram, C. F. Johnston, J. L. Hollander, M. J. Kappers, C. J. Humphreys, *J. Appl. Phys.* 105 (11) (2009) 113501–7. doi:10.1063/1.3129307.
- ¹⁴C. Q. Chen, V. Adivarahan, M. Shatalov, M. E. Gaevski, E. Kuokstis, J. W. Yang, H. P. Maruska, Z. Gong, M. A. Khan, R. Liu, A. Bell, F. A. Ponce, *Phys. Status Solidi C* 2 (7) (2005) 2732–2735. doi:10.1002/pssc.200461547.
- ¹⁵C.-H. Lin, S. Tamaki, Y. Yamashita, H. Miyake, K. Hiramatsu, *Appl. Phys. Express* 9 (8) (2016) 081001. doi:10.7567/APEX.9.081001.
- ¹⁶C.-H. Lin, Y. Yamashita, H. Miyake, K. Hiramatsu, *J. Cryst. Growth* 468 (2017) 845–850. doi:10.1016/j.jcrysgro.2016.09.076.
- ¹⁷D. V. Dinh, N. Hu, Y. Honda, H. Amano, M. Pristovsek, *J. Cryst. Growth* 498 (2018) 377–380. doi:10.1016/j.jcrysgro.2018.07.015.
- ¹⁸D. V. Dinh, H. Amano, M. Pristovsek, *J. Cryst. Growth* 502 (2018) 14–18. doi:10.1016/j.jcrysgro.2018.09.001.
- ¹⁹M. R. Laskar, T. Ganguli, A. A. Rahman, A. P. Shah, M. R. Gokhale, A. Bhattacharya, *Phys. Status Solidi (RRL)* 4 (7) (2010) 163–165. doi:10.1002/pssr.201004091.
- ²⁰S. C. Choi, J.-H. Kim, J. Y. Choi, K. J. Lee, K. Y. Lim, G. M. Yang, *J. Appl. Phys.* 87 (1) (1999) 172–176. doi:10.1063/1.371840.
- ²¹A. A. Allerman, M. H. Crawford, A. J. Fischer, K. H. A. Bogart, S. R. Lee, D. M. Follstaedt, P. P. Provencio, D. D. Koleske, *J. Cryst. Growth* 272 (1) (2004) 227–241. doi:10.1016/j.jcrysgro.2004.08.035.
- ²²A. V. Lobanova, K. M. Mazaev, R. A. Talalaev, M. Leys, S. Boeykens, K. Cheng, S. Degroote, *J. Cryst. Growth* 287 (2) (2006) 601–604. doi:10.1016/j.jcrysgro.2005.10.083.
- ²³B. Neuschl, J. Helbing, M. Knab, H. Lauer, M. Madel, K. Thonke, T. Meisch, K. Forghani, F. Scholz, M. Feneberg, *J. Appl. Phys.* 116 (11) (2014) 113506–8. doi:10.1063/1.4895995.
- ²⁴H. Zhou, S. J. Chua, C. Peng, *J. Cryst. Growth* 292 (1) (2006) 5–9. doi:10.1016/j.jcrysgro.2006.03.055.
- ²⁵J. Stellmach, F. Mehnke, M. Frentrup, C. Reich, J. Schlegel, M. Pristovsek, T. Wernicke, M. Kneissl, *J. Cryst. Growth* 367 (2013) 42–47. doi:10.1016/j.jcrysgro.2013.01.006.
- ²⁶M. Feneberg, M. Winkler, J. Klamsner, J. Stellmach, M. Frentrup, S. Ploch, F. Mehnke, T. Wernicke, M. Kneissl, R. Goldhahn, *Appl. Phys. Lett.* 106 (18) (2015) 182102–4. doi:10.1063/1.4920985.
- ²⁷M. R. Laskar, T. Ganguli, A. A. Rahman, A. Mukherjee, N. Hattui, M. R. Gokhale, A. Bhattacharya, *J. Appl. Phys.* 109 (1) (2011) 013107–8. doi:10.1063/1.3525602.
- ²⁸G. T. Wang, J. R. Creighton, *J. Phys. Chem. A* 110 (3) (2005) 1094–1099. doi:10.1021/jp054133o.
- ²⁹L. Lymperakis, J. Neugebauer, *Phys. Rev. B* 79 (24) (2009) 241308. doi:10.1103/PhysRevB.79.241308.
- ³⁰C. Buchheim, R. Goldhahn, M. Rakel, C. Cobet, N. Esser, U. Rossow, D. Fuhrmann, A. Hangleiter, *Phys. Status Solidi B* 242 (13) (2005) 2610–2616. doi:10.1002/pssb.200541265.
- ³¹C. Coughlan, S. Schulz, M. A. Caro, E. P. O’Reilly, *Phys. Status solidi B* 252 (5) (2015) 879–884. doi:10.1002/pssb.201451593.
- ³²Y. Koide, H. Itoh, M. R. H. Khan, K. Hiramatsu, N. Sawaki, I. Akasaki, *J. Appl. Phys.* 61 (9) (1998) 4540–4543. doi:10.1063/1.338387.